Charge disproportionation and metal-insulator transition in the quasi-one-dimensional conductor β-$Na_{0.33}V_2O_5$: ^{23}Na NMR study of a single crystal

Masayuki Itoh, Ichihiro Yamauchi, Tomokazu Kozuka, and Tomoyuki Suzuki
Department of Physics, Graduate School of Science, Nagoya University, Furo-cho, Chikusa-ku, Nagoya 464-8602, Japan

Touru Yamauchi, Jun-Ichi Yamaura, and Yutaka Ueda
Institute for Solid State Physics, University of Tokyo, Kashiwanoha, Kashiwa 277-8581, Japan
(Received 5 March 2006; published 30 August 2006)

^{23}Na NMR measurements have been made on a single crystal to study the charge disproportionation accompanied by the metal-insulator transition in the quasi-one-dimensional conductor β-$Na_{0.33}V_2O_5$. We observed one set of ^{23}Na NMR spectrum split by an electric quadrupole interaction in the metallic phase with the Na disordering, two sets in the metallic phase with the Na ordering, and six sets in the insulating phase. These observations are concluded to be consistent with the lattice symmetry proposed by the x-ray diffraction and the neutron scattering studies. The angular dependences of the ^{23}Na Knight shift have been measured in the three phases. From the analysis of the angular dependences based on the local magnetic susceptibilities in the metallic phases determined by the ^{51}V NMR study, we can clearly conclude that the V1 site is the most magnetic. Furthermore, comparing those with the calculated curves based on several models of the charge ordering and the charge disproportionation in the insulating phase, we find that the metal-insulator transition is accompanied not by the charge ordering of V^{4+} and V^{5+} but by the charge disproportionation. We propose a model of the charge disproportionation consistent with the spin structure in the antiferromagnetic state. A model of the electronic structure in the β-$Na_{0.33}V_2O_5$ is also discussed from the aspect of the metal-insulator transition.

DOI: 10.1103/PhysRevB.74.054434 PACS number(s): 71.30.+h, 75.25.+z, 76.60.Cq, 76.60.Gv

I. INTRODUCTION

In transition metal oxides, charge degrees of freedom have been extensively discussed from various aspects of phenomena such as the charge stripe in cuprates and nickelates, the charge nanoscopic modulation of the charge and spin density related to the colossal magnetoresistance in manganites, and so on.[1] Among them, the vanadium bronzes $A_xV_2O_5$ (A=alkali, alkaline earth, and metals) have been investigated on the charge ordering (CO) after the discovery of the CO transition in α'-NaV_2O_5.[2,3] Recently, the vanadium bronze β-$Na_{0.33}V_2O_5$, a mixed-valence oxide of V^{4+} ($3d^1$) and V^{5+} ($3d^0$), was reported to have a superconducting phase around ~8 GPa below ~9 K.[4–6] The superconductivity, that appears when the CO is suppressed by applying pressure, has attracted much attention from the viewpoint of the superconducting mechanism due to the charge fluctuations. In ambient pressure, this oxide successively undergoes phase transitions, namely, an ordering of Na atoms at T_{Na} ~242 K, a metal-insulator (MI) transition at T_{MI} ~135 K, and an antiferromagnetic (AF) transition at T_N ~24 K.[7–9] The electron filling, the CO pattern, and the MI transition mechanism closely related to the superconducting mechanism in β-$Na_{0.33}V_2O_5$ have not been clarified even in ambient pressure, though it is desired to understand the superconducting mechanism.

β-$Na_{0.33}V_2O_5$ is crystallized into a monoclinic structure (the lattice symmetry $C2/m$) at room temperature.[10] There are three vanadium sites, V1, V2, and V3. The V1 and V3 sites form zigzag chains of edge sharing VO_6 octahedra and VO_5 pyramids, respectively, along the b axis, whereas the V2 sites lie on ladders of corner sharing of VO_6 octahedra along the b axis. Na atoms are located at the A1 sites in a tunnel of the V_2O_5 framework. The neighboring two Na sites are too close to be simultaneously occupied by Na atoms, leading to the stoichiometric concentration of $x=1/3$ in the β structure. The Na atoms are randomly occupied above T_{Na} and the Na ordering takes place below T_{Na}.[7,11,12] The lattice symmetry was reported to change from $C2/m$ to $P2_1/a$ at T_{Na} due to the Na ordering, resulting in the unit cell of $a \times 2b \times c$, whereas each V site is split into two sites, V(A) and V(B).[11,12] Below T_{MI}, the crystallographically inequivalent three Na sites, Na(A), Na(B), and Na(C), appear due to the $6b$ lattice modulation along the b axis without a change of the lattice symmetry, while each V site is split into six sites, V(A)–V(F).

In the β structure with $x=1/3$, the nominal ratio of V^{4+} to V^{5+} is 1:5. Therefore, if V^{4+} is located at the V1 or the V3 sites, this oxide is a quarter-filled zigzag chain system. It becomes a quarter-filled two-leg ladder system, if V^{4+} occupies the V2 sites. Okazaki *et al.*, however, showed that the quarter-filled ladder or chain model cannot explain the results of the angle-resolved photoemission spectroscopy in the metallic phase.[13] Based on extended Hückel tight-binding calculations for an isomorphous oxide β-$Sr_{0.33}V_2O_5$, Doublet and Lepetit proposed weakly interacting two-leg ladders composed of two V1-V3 and one V2-V2 ladders in contrast with the model with two zigzag chains and a two-leg ladder.[14] Recently we made the detailed ^{51}V NMR measurements on a single crystal to study the local magnetic susceptibilities of β-$Na_{0.33}V_2O_5$.[15] We estimated the $3d$ electron numbers at the V1, V2, and V3 sites from the ^{51}V Knight shifts and proposed a model of the electronic structure in the metallic phases on the basis of the weakly coupled two-leg ladders.

One of the most interesting issues in β-$Na_{0.33}V_2O_5$ is the CO or the charge disproportionation (CD) which leads to the MI transition. Several models have been discussed on the CO or the CD pattern. In the previous NMR studies, we proposed the chain models where V^{4+} ions are located at half of the V1 or the V2 sites, and the zigzag model of V^{4+} located at half of the V2 ladder sites.[16,17] Nishimoto and Ohta showed from the Madelung potential calculations that the V1 sites are occupied by V^{4+}.[18] After these studies, Yamaura *et al.* found in x-ray diffraction measurements the $2b$ modulation due to the Na ordering below T_{Na} and the $6b$ modulation accompanied by the CO transition below T_{MI}.[11] They proposed the rectangle type of CO with the V sites on the V2 ladder. Heinrich *et al.* concluded from ESR measurements that $3d$ electrons are located on the V1 zigzag chains.[19] Phuoc *et al.* discussed the x (x=0.5–1) variation of the CO pattern in $A_xV_6O_{15}$ (A=Na and Sr) from the optical measurements.[20] On the other hand, Nagai *et al.* found by the neutron scattering measurements that the amplitudes of the magnetic moments at the V sites in the three types of V-O chains are modulated with a period of $3b$ along the b axis below T_N.[12] They proposed that the CD occurs with a period of $3b$, not $6b$, and that the $6b$ lattice modulation below T_{MI} is attributed to an instability in the V $3d$ band to form $3b$ charge modulation on the preexistent $2b$ lattice modulation. Thus what happens in the insulating phase, the CO or the CD, remains controversial.

^{23}Na NMR measurements are expected to be useful in knowing the CO or the CD pattern, because a classical dipole interaction between a sodium nucleus and the vanadium magnetic moments, which is closely related to the CO or the CD pattern, governs a local magnetic field at the sodium site. In this study we have made ^{23}Na NMR measurements on a single crystal to investigate the CO or the CD accompanied by the MI transition in β-$Na_{0.33}V_2O_5$. We will determine the ^{23}Na electric field gradient (EFG) tensor in the metallic and insulating phases and will discuss it on the basis of the site symmetry. From the analysis of the anisotropy of the ^{23}Na Knight shift K, we will find that the V1 site is the most magnetic in both the metallic and the insulating phases. Also comparing the angular dependences of K with the calculated ones based on several CO and CD models, we will show that the MI transition is accompanied not by the CO of V^{4+} and V^{5+} but by the CD. We will propose a CD model consistent with the spin structure in the AF state. A model of the electronic structure in the β-$Na_{0.33}V_2O_5$ will be also proposed and discussed from the aspect of the MI transition.

II. EXPERIMENTAL PROCEDURE

Single crystals of β-$Na_{0.33}V_2O_5$ were prepared by an rf heating Czochralski method using $NaVO_3$ as a solvent in a Pt crucible.[4] We used the same crystal of $0.5\times2.8\times0.9$ mm^3 as that in the ^{51}V NMR experiments.[15] NMR measurements were made using a coherent pulsed spectrometer and a superconducting magnet with a constant field of H_0=5.8710 T. ^{23}Na Fourier-transformed (FT) NMR spectra for spin echo signals were taken with the sample rotated in the field.

Since the results in the next section are obtained from analyzing in detail NMR spectra, it will be useful to summarize the basic formula used in the next section. The Hamiltonian of a ^{23}Na nucleus with the nuclear spin $\mathbf{I}$ (^{23}I=3/2) and the nuclear gyromagnetic ratio γ_n at a sodium site in β-$Na_{0.33}V_2O_5$ is expressed as (Ref. 21)

$$H = -\gamma_n\hbar\mathbf{I}\cdot(\mathbf{1}+\mathbf{K}+\mathbf{K}_D+\mathbf{K}_L+\mathbf{K}_C)\cdot\mathbf{H_0}+\sum_{\alpha\beta}V_{\alpha\beta}Q_{\alpha\beta}, \tag{1}$$

where $\hbar$ is the Planck's constant divided by 2π and the first term with the unit tensor $\mathbf{1}$ is the Zeeman interaction due to the external field $\mathbf{H_0}$. Also $\mathbf{K}$, $\mathbf{K}_D$, $\mathbf{K}_L$, and $\mathbf{K}_C$ are the Knight shift tensors due to the local field coming from the vanadium magnetic moments $\mathbf{H}_{loc}$, the demagnetization field $\mathbf{H}_D$, the Lorentz field $\mathbf{H}_L$, and the chemical shift tensor, respectively. The last term is the electric quadrupole interaction between the EFG tensor $V_{\alpha\beta}$ and the nuclear quadrupole moment $eQ_{\alpha\beta}$.

The electric quadrupole interaction leads to three lines, one central and two satellite ones, in the ^{23}Na NMR spectrum. We consider the case of $H_0\perp a^*$, the axis perpendicular to the b and c axes in the monoclinic structure, and measure the angle of H_0 rotation, θ_{a^*}, in the bc plane from the position in which the b axis coincides with H_0. In the first-order perturbation, where the electric quadrupole interaction is much smaller than the Zeeman one, the difference between resonance frequencies of the $3/2\leftrightarrow1/2$ and $-1/2\leftrightarrow-3/2$ satellite transitions, $\delta\nu_{3/2\leftrightarrow1/2}$, is expressed as follows (Ref. 22):

$$\delta\nu_{3/2\leftrightarrow1/2}=\nu_{1,a^*}+\nu_{2,a^*}\cos2\theta_{a^*}+\nu_{3,a^*}\sin2\theta_{a^*} \tag{2}$$

with

$$\nu_{1,a^*}=\nu_Q(V_{bb}+V_{cc})/V_{ZZ},$$

$$\nu_{2,a^*}=\nu_Q(V_{bb}-V_{cc})/V_{ZZ},$$

$$\nu_{3,a^*}=-2\nu_QV_{bc}/V_{ZZ}, \tag{3}$$

and

$$\nu_Q=\frac{3eQV_{ZZ}}{2I(2I-1)h}, \tag{4}$$

where ν_Q is the electric quadrupole frequency, $V_{\alpha\beta}$ (α, β $=a^*$, b, and c) are components of the EFG tensor, V_{ZZ} is the Z principal component of the tensor, and $eQ=eQ_{ZZ}$. Similar relations for H_0 rotations in the ca^* and a^*b planes are obtained by cyclic permutation. In this procedure one can subtract the Knight shift. After determining the EFG tensor components in the ca^*b coordinate system with Eqs. (2)–(4), one can obtain the X, Y, and Z principal components and the principal axes X_Q, Y_Q, and Z_Q by diagonalizing the EFG tensor. The principal components and axes are useful in knowing the site symmetry at the Na sites. Also one can determine ν_Q and the asymmetry parameter of the EFG, η $=|V_{XX}-V_{YY}|/|V_{ZZ}|$ ($|V_{XX}|\leq|V_{YY}|\leq|V_{ZZ}|$).

The Knight shift due to H_{loc}, K, in the ^{23}Na NMR spectrum is useful in obtaining information on the CO or the CD pattern. When K is very small and comparable to K_D, K_L, K_C, and the second-order quadrupole effect, one has to make these corrections for the resonance frequency of the central line, $\nu_{1/2\leftrightarrow -1/2}$. The angular dependence of $\nu_{1/2\leftrightarrow -1/2}$ due to the second-order electric quadrupole effect can be calculated from the equations given in Ref. 23. $\mathbf{H}_D$ is evaluated as $\mathbf{H}_D = -\chi \mathbf{N} \cdot \mathbf{H}_0$ where $\mathbf{N}$ is the demagnetization factor tensor and χ is magnetic susceptibility. Also $\mathbf{H}_L$ can be calculated as $\mathbf{H}_L = \frac{4\pi}{3}\chi \mathbf{H}_0$. Using the resonance frequency ν_1 after correcting the second-order electric quadrupole effect, K_D, and K_L for $\nu_{1/2\leftrightarrow -1/2}$, we define the ^{23}Na Knight shift K as $K = (\nu_1 - \nu_0)/\nu_0$, where ν_0 (=66.1165 MHz) is the ^{23}Na resonance frequency in aqueous $NaVO_3$ solution, to subtract K_C. Thus we can obtain K due to only H_{loc}. When H_0 is rotated in the bc plane, K is expressed as

$$K = k_{1,a^*} + k_{2,a^*} \cos 2\theta_{a^*} + k_{3,a^*} \sin 2\theta_{a^*} \tag{5}$$

with

$$k_{1,a^*} = (K_{bb} + K_{cc})/2,$$

$$k_{2,a^*} = (K_{bb} - K_{cc})/2,$$

$$k_{3,a^*} = K_{bc}, \tag{6}$$

where $K_{\alpha\beta}$ (α, $\beta = a^*$, b, and c) are components of the K tensor. Similar relations for H_0 rotations in the ca^* and a^*b planes are obtained by cyclic permutation. After determining the K tensor components in the ca^*b coordinate system from Eqs. (5) and (6), one can obtain the X, Y, and Z principal components, K_X, K_Y, and K_Z, and also the principal axes X_K, Y_K, and Z_K by diagonalizing the K tensor.

III. EXPERIMENTAL RESULTS

A. Electric field gradient

Above T_{Na}, we observed one set of ^{23}Na FT NMR spectrum, S, with one central and two satellite lines split by the electric quadrupole interaction in β-$Na_{0.33}V_2O_5$ as seen in Fig. 1 where the ^{23}Na FT NMR spectrum with H_0 parallel to the direction of $\theta_c = 72^\circ$ in the a^*b plane at 300 K is presented with the spectra at 150 and 40 K. Figure 2 shows the angular dependence of the ^{23}Na resonance frequency, ν_{res}, with H_0 rotated in the bc, ca^*, and a^*b planes at 300 K in β-$Na_{0.33}V_2O_5$. The observed angular dependence of ν_{res} is well explained by Eqs. (2)–(4) with the values of ν_Q and η as listed in Table I. The Z_Q axis is the b axis, whereas the X_Q axis is located at the angle of -150.0° from the c axis in the ca^* plane, namely, $(\theta, \phi) = (90.0^\circ, -150.0^\circ)$ where the polar angle θ and the azimuthal angle ϕ are introduced to define the direction of the principal axis of the EFG tensor in the ca^*b coordinate system. The experimental error of the angles is about in $\pm 1^\circ$.

In the T range $T_{MI} \leqslant T \leqslant T_{Na}$, we observed two sets of ^{23}Na NMR spectra, S1 and S2, split by the electric quadrupole interaction as seen in Fig. 1. Figure 3 shows the angular dependence of ν_{res} of the S1 and S2 spectra at 150 K. The angular dependence is very slightly split into two sets for the H_0 rotation in the bc plane and clearly for the rotation in the a^*b plane, whereas only one set is observed for $H_0 \| b$ and $H_0 \perp b$, as seen in Fig. 3. Fitting these experimental results to Eqs. (2)–(4), we obtained the ν_Q and η values with the directions of the Z_Q and X_Q axes for the S1 and S2 spectra as listed in Table I. It should be noted that the two ^{23}Na NMR spectra have the same values of ν_Q and η, whereas the Z_Q axes of the two spectra slightly deviate from the b axis to the different directions.

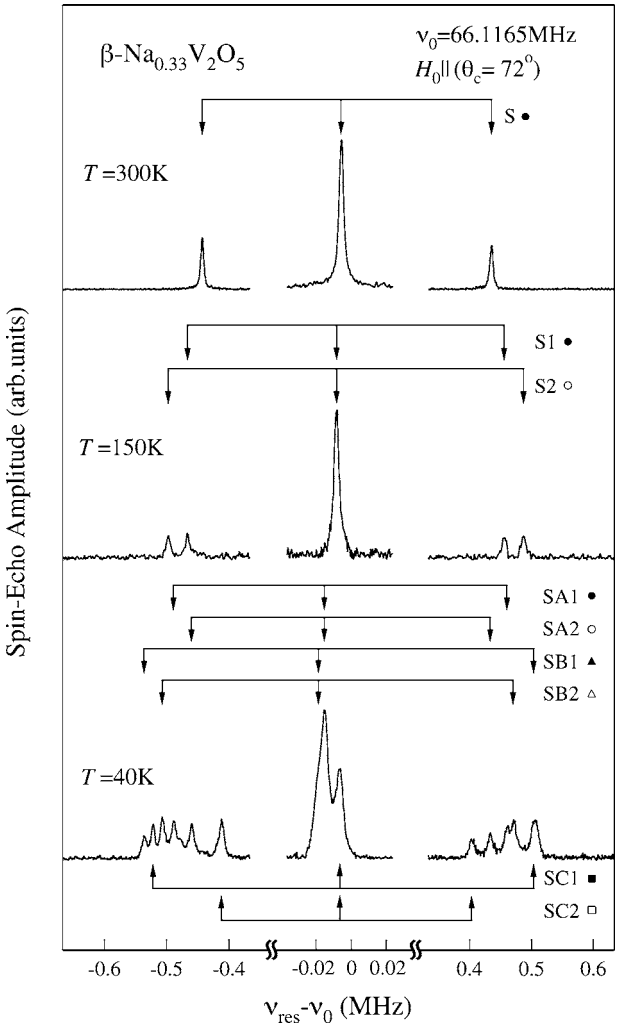

FIG. 1. ^{23}Na FT NMR spectra at 300, 150, and 40 K with H_0 (=5.8710 T) applied parallel to the direction of $\theta_c = 72^\circ$ in the a^*b plane of β-$Na_{0.33}V_2O_5$. ν_{res} and ν_0 (=66.1165 MHz) are ^{23}Na resonance frequencies in β-$Na_{0.33}V_2O_5$ and aqueous $NaVO_3$ solution, respectively. The symbols of S, S1, S2, SA1, SA2, SB1, SB2, SC1, and SC2 with the arrows denote the ^{23}Na NMR spectra split by an electric quadrupole interaction.

Below T_{MI}, we observed six sets of NMR spectra, SA1, SA2, SB1, SB2, SC1, and SC2 as seen in Fig. 1. The angular dependences of ν_{res} at 40 K are presented in Fig. 4. Six sets are seen for H_0 rotations in the a^*b and bc planes, while three sets appear for $H_0 \perp b$ and $H_0 \| b$. From the same fitting as mentioned above, we obtained the ν_Q and η values with

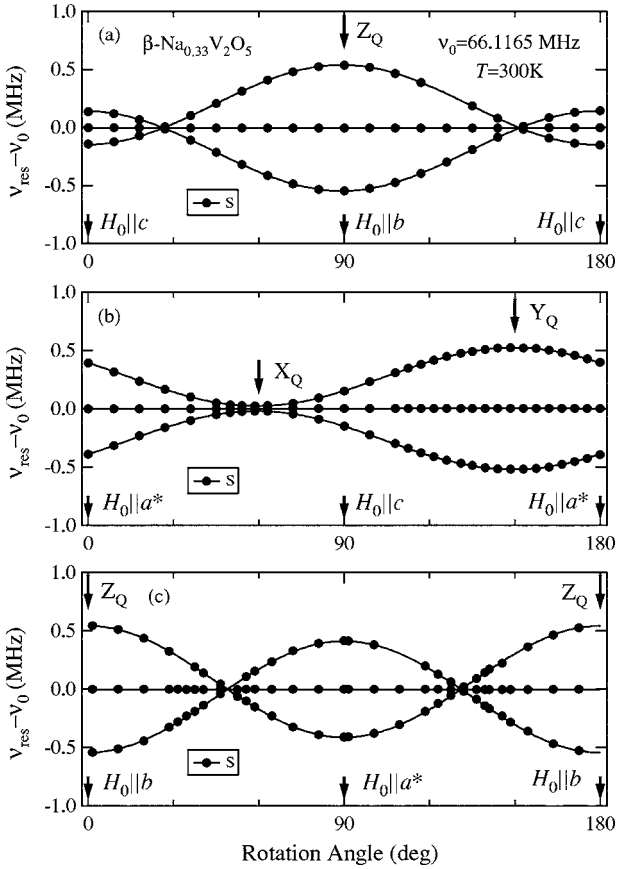

FIG. 2. Angular dependence of the ^{23}Na resonance frequency ν_{res} of the S spectrum at 300 K with H_0 (=5.8710 T) rotated in the (a) bc, (b) ca^*, and (c) a^*b planes of β-$Na_{0.33}V_2O_5$. The solid curves represent fitted results of the data to Eqs. (2)–(4) with the ν_Q and η parameters (see Table I). ν_0 (=66.1165 MHz) is the ^{23}Na resonance frequency in aqueous $NaVO_3$ solution. The symbols of X_Q, Y_Q, and Z_Q with the arrows are principal axes of the EFG tensor in the ^{23}Na NMR spectrum.

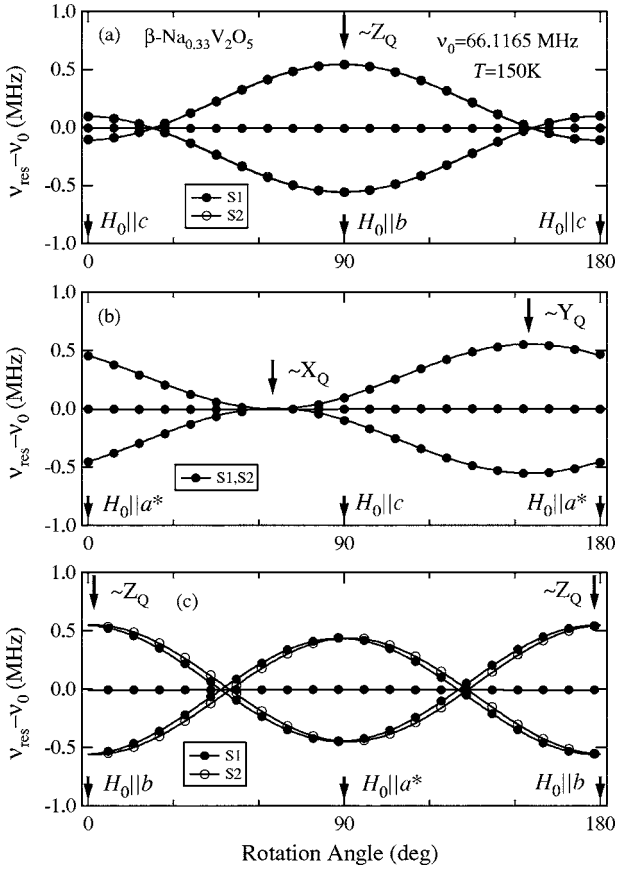

FIG. 3. Angular dependence of the ^{23}Na resonance frequency ν_{res} of the S1 and S2 spectra at 150 K with H_0 (=5.8710 T) rotated in the (a) bc, (b) ca^*, and (c) a^*b planes of β-$Na_{0.33}V_2O_5$. The solid curves represent fitted results of the data to Eqs. (2)–(4) with the ν_Q and η parameters (see Table I). ν_0 (=66.1165 MHz) is the ^{23}Na resonance frequency in aqueous $NaVO_3$ solution. The symbols of X_Q, Y_Q, and Z_Q with the arrows are principal axes of the EFG tensors in the ^{23}Na NMR spectra.

the directions of Z_Q and X_Q for the six spectra as listed in Table I. The six spectra can be classified into three groups, ($SA1$,$SA2$), ($SB1$,$SB2$), and ($SC1$,$SC2$). The two spectra in each group have almost the same values of ν_Q and η, while the directions of the principal axes are different from each other.

Figure 5 shows the T dependences of ν_Q ($=\nu_Q^Z$) and ν_Q^Y [$=3eQV_{YY}/2I(2I-1)h$] for the S spectrum above T_{Na}, the S1 and S2 spectra in the T range $T_{MI} \leqslant T \leqslant T_{Na}$, and the $SA1$, $SA2$, $SB1$, $SB2$, $SC1$, and $SC2$ spectra below T_{MI}. In the metallic phases, both ν_Q and ν_Q^Y, which are the same for the S1 and S2 spectra, increase with decreasing T. The Z_Q axis is

TABLE I. The ^{23}Na electric quadrupole frequency ν_Q, the asymmetry parameter of the electric field gradient (EFG) η, and the directions of the principal Z_Q and X_Q axes of the EFG tensors at 300, 150, and 40 K in $\beta-Na_{0.33}V_2O_5$.

T (K)	Spectrum	ν_Q (MHz)	η	Z_Q ($\theta°$,$\phi°$)	X_Q ($\theta°$,$\phi°$)
300	S	0.543	0.969	(0.0, -)	(90.0, −150.0)
150	S1	0.552	0.995	(1.6,−81.5)	(89.5, 25.4)
	S2	0.552	0.995	(177.8,−120.0)	(88.2,−154.7)
40	$SA1$	0.552	0.968	(91.0, 115.9)	(94.9, 25.8)
	$SA2$	0.551	0.967	(89.0, 116.1)	(92.8,−153.9)
	$SB1$	0.591	0.964	(5.8, 29.3)	(95.8, 21.4)
	$SB2$	0.592	0.963	(175.4, 36.3)	(94.5,−158.5)
	$SC1$	0.566	0.975	(94.3, 113.8)	(96.8, 23.2)
	$SC2$	0.565	0.971	(85.4, 114.0)	(95.4,−156.4)

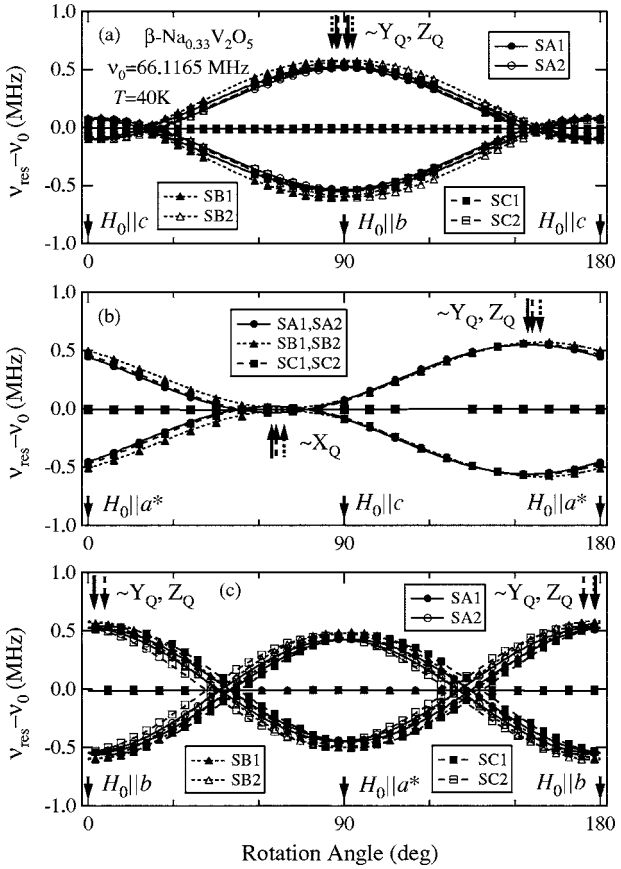

FIG. 4. Angular dependence of the ^{23}Na resonance frequency ν_{res} of the SA1, SA2, SB1, SB2, SC1, and SC2 spectra at 40 K with H_0 (=5.8710 T) rotated in the (a) bc, (b) ca^*, and (c) a^*b planes of β-$Na_{0.33}V_2O_5$. ν_0 (=66.1165 MHz) is the ^{23}Na resonance frequency in aqueous $NaVO_3$ solution. The curves represent fitted results of the data to Eqs. (2)–(4) with the ν_Q and η parameters (see Table I). The symbols of X_Q, Y_Q, and Z_Q with the arrows are principal axes of the EFG tensors in the ^{23}Na NMR spectra.

located near the b axis and $\eta \sim 1$. Below T_{MI}, however, we observed three sets of ν_Q and ν_Q^Y for the three groups of (SA1,SA2), (SB1,SB2), and (SC1,SC2) spectra. It should be noted that $Y_Q \sim b$ for the SA1, SA2, SC1, and SC2 spectra

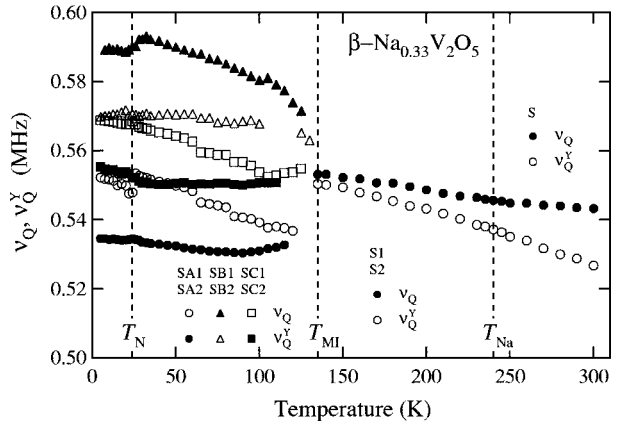

FIG. 5. Temperature dependence of the ^{23}Na electric quadrupole frequencies ν_Q (=ν_Q^Z) and ν_Q^Y for the S, S1, S2, SA1, SA2, SB1, SB2, SC1, and SC2 spectra in β-$Na_{0.33}V_2O_5$.

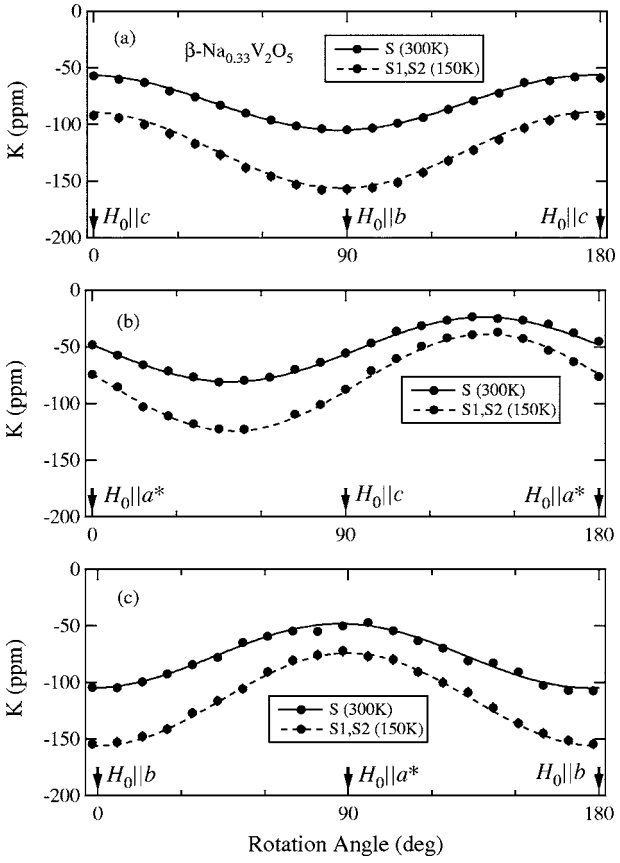

FIG. 6. Angular dependence of K of the ^{23}Na NMR spectra, S, at 300 K and, S1 and S2, at 150 K with H_0 rotated in the (a) bc, (b) ca^*, and (c) a^*b planes of β-$Na_{0.33}V_2O_5$. The solid and dashed curves represent the fitted results of the experimental data to Eqs. (5) and (6) with the Knight shift parameters listed in Table II.

below $\sim T_{MI}$, that is, the Z_Q axis is exchanged with the Y_Q axis below T_{MI}, whereas $Z_Q \sim b$ for the SB1 and SB2 spectra even below T_{MI}.

B. Knight shift

In the present case, we have to make several corrections to obtain the Knight shift due to the local magnetic field, K, as mentioned in Sec. II, since the absolute value of K is very small. We calculated the second-order electric quadrupole effect on $\nu_{1/2\leftrightarrow -1/2}$, using the experimental values listed in Table I and the equations given in Ref. 23. Also, using the χ data in Ref. 16 and assuming a column with $3 \leqslant k_0 \leqslant 5$ for the present sample where k_0 is the ratio of length to diameter, we estimated for example -39.2 ppm$\leqslant K_D \leqslant -37.5$ ppm for $H_0 \perp b$ and K_L=27.2 ppm at 300 K. After subtracting the second-order electric quadrupole effect, K_D, K_L, and K_C from $\nu_{1/2\leftrightarrow -1/2}$, we obtained K. Figure 6 shows the angular dependences of K with H_0 rotated in the bc, ca^*, and a^*b planes at 300 and 150 K in β-$Na_{0.33}V_2O_5$. Fitting the experimental data at 300 K to Eqs. (5) and (6), we obtained the isotropic ^{23}Na Knight shift $K_{iso}=(K_X+K_Y+K_Z)/3$, the axial shift $K_{ax}=(2K_Z-K_X-K_Y)/6$, and the anisotropic shift $K_{aniso}=(K_Y-K_X)/2$ with the directions of the Z_K and X_K axes as listed in

TABLE II. ^{23}Na Knight shifts K_{iso}, K_{ax}, and K_{aniso} at 300, 150, and 40 K in β-$Na_{0.33}V_2O_5$. The directions of the Z_K and X_K axes of the Knight shift tensors are also listed.

T (K)	Spectrum	K_{iso} (ppm)	K_{ax} (ppm)	K_{aniso} (ppm)	Z_K (θ°, ϕ°)	X_K (θ°, ϕ°)
300	S	−70	−18	−28	(7.9, 135.8)	(89.5, −130.9)
150	S1, S2	−106	−25	−43	(4.0, 148.9)	(90.6, −130.0)
40	*SA*1, *SA*2	−168	−55	−60	(178.1, −13.9)	(89.0, 45.8)
	*SB*1, *SB*2	−210	−55	−124	(176.4, −15.3)	(91.1, −122.7)
	*SC*1, *SC*2	−125	−27	−39	(84.0, 137.2)	(89.1, −132.7)

Table II. In the T range $T_{MI} \leqslant T \leqslant T_{Na}$, we observed one central line as seen in Fig. 6. This means that two sets of NMR spectra, S1 and S2, have the same K. The values of K_{iso}, K_{ax}, and K_{aniso} at 150 K are listed with the directions of the Z_K and X_K axes in Table II. In the T range $T_N < T < T_{MI}$, we observed three central lines coming from the three groups of (*SA*1, *SA*2), (*SB*1, *SB*2), and (*SC*1, *SC*2). This shows that the two spectra in each of the three groups have the same K tensor. Figure 7 shows the angular dependences of K at 40 K. The obtained Knight shifts of (*SA*1, *SA*2), (*SB*1, *SB*2), and (*SC*1, *SC*2) are listed with the directions of the principal axes in Table II.

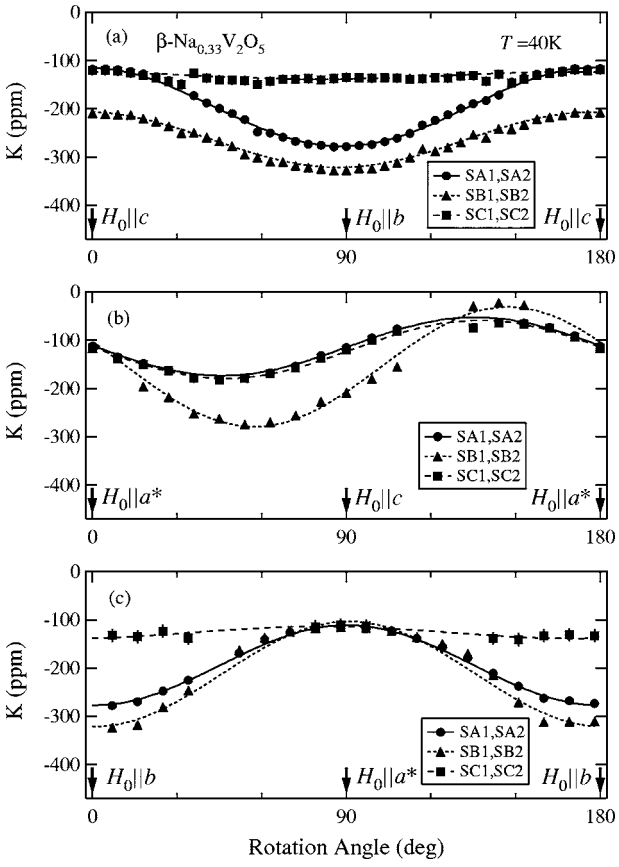

FIG. 7. Angular dependence of K of the ^{23}Na NMR spectra, *SA*1, *SA*2, *SB*1, *SB*2, *SC*1, and *SC*2, at 40 K with H_0 rotated in the (a) bc, (b) ca^*, and (c) a^*b planes of β-$Na_{0.33}V_2O_5$. The solid, dashed, and dotted curves represent the fitted results of the experimental data to Eqs. (5) and (6) with the Knight shift parameters listed in Table II.

We measured the T dependences of $\nu_{res} - \nu_0$ for the central lines with H_0 parallel to the X_K, Y_K, and Z_K principal axes of the K tensor. The results are presented in Fig. 8. We observed one central line in the metallic phases and three below T_{MI}. Also it should be noted that the Z_K axis is exchanged with the Y_K axis below T_{MI} only in the *SC*1 and *SC*2 spectra. In the AF phase, we could not make a site assignment for the spectra represented by the open symbols in Fig. 8. The T dependences of $\nu_{res} - \nu_0$ below T_N follow the T dependence of the sublattice magnetization. Figure 9 shows the T dependences of K_{iso}, K_{ax}, and K_{aniso} above T_N after correcting the

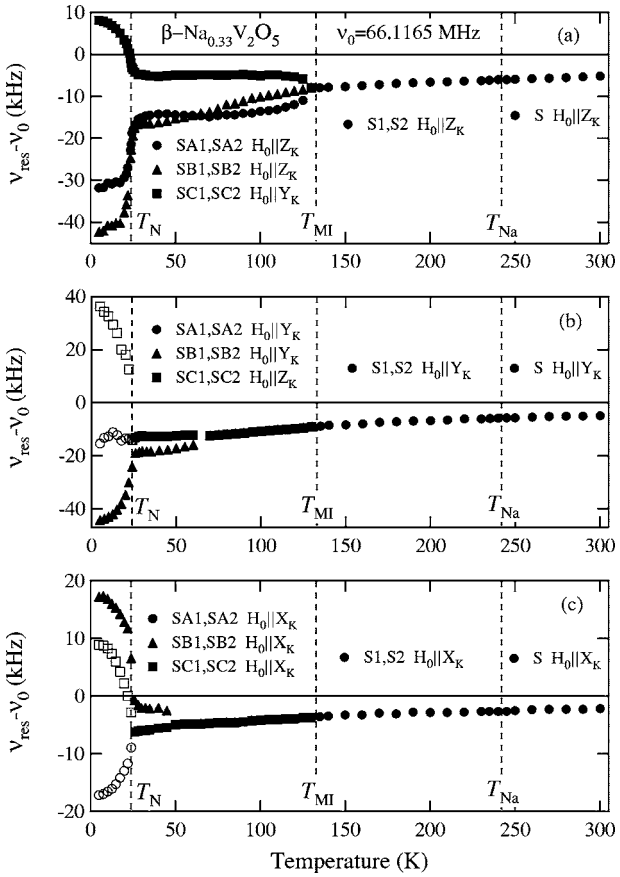

FIG. 8. Temperature dependence of the ^{23}Na resonance frequency of the central line $\nu_{res} - \nu_0$ with H_0 parallel to the (a) Z_K (Y_K), (b) Y_K (Z_K), and (c) X_K axes of the S, S1, S2, *SA*1, *SA*2, *SB*1, and *SB*2 (*SC*1 and *SC*2) spectra in β-$Na_{0.33}V_2O_5$ where ν_0(=66.1165 MHz) is the ^{23}Na resonance frequency in aqueous $NaVO_3$ solution. A site assignment of the open symbols is not made below T_N.

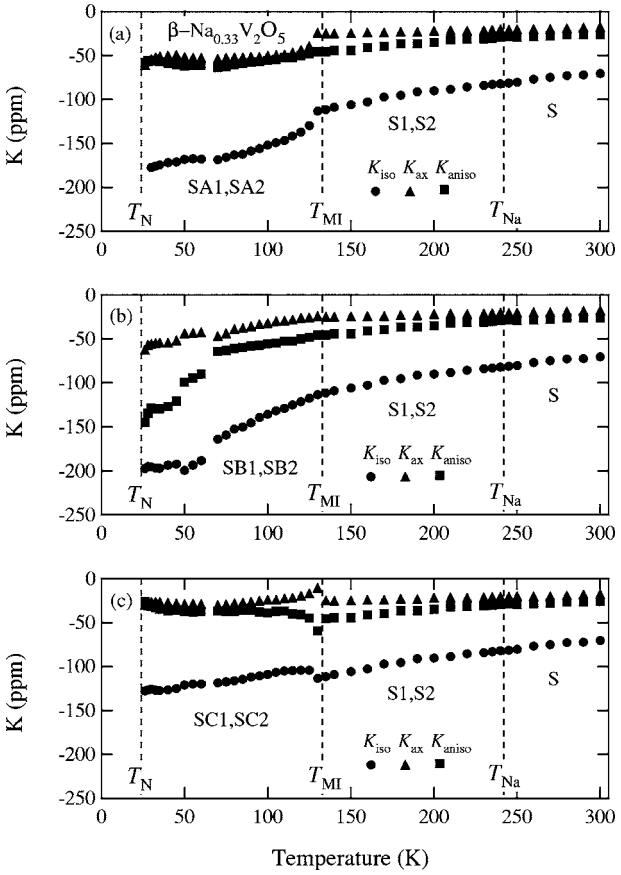

FIG. 9. Temperature dependence of the ^{23}Na isotropic Knight shift K_{iso}, the axial shift K_{ax}, and the anisotropic shift K_{aniso} for (a) the S, S1, S2, SA1, and SA2 spectra, (b) the S, S1, S2, SB1, and SB2 spectra, and (c) the S, S1, S2, SC1, and SC2 spectra in β-$Na_{0.33}V_2O_5$. For comparison, the data of the S, S1, and S2 spectra are included in (b) and (c).

second-order electric quadrupole effect, K_D, and K_L for the experimental data in Fig. 8. The Knight shifts monotonically decrease with decreasing T in the metallic phases. Also the T dependences of these Knight shifts follow the magnetic susceptibility, which obeys the Curie Weiss law,[15,16] as shown in Fig. 10 where the Knight shifts versus χ plots are presented with T as an implicit parameter in the metallic phases. The slopes of the straight lines in Fig. 10 provide the isotropic hyperfine coupling constant A_{hf}^{iso}, the axial one A_{hf}^{ax}, and the anisotropic one A_{hf}^{aniso} as −2.35, −0.41, and −1.21 kOe/μ_B, respectively.

IV. ANALYSIS AND DISCUSSION

A. Na spectrum and site symmetry

We discuss the relation between the observed ^{23}Na NMR spectra and the site symmetry. X-ray diffraction[11] and neutron scattering[12] studies proposed that the crystal symmetry of β-$Na_{0.33}V_2O_5$ is $C2/m$ above T_{Na} and $P2_1/a$ below T_{Na}. Figures 11(a)–11(c) show the projection of the Na sites on the bc plane in the T ranges, $T > T_{Na}$, $T_{MI} \leqslant T \leqslant T_{Na}$, and $T < T_{MI}$, respectively. In Fig. 11, the large and small circles

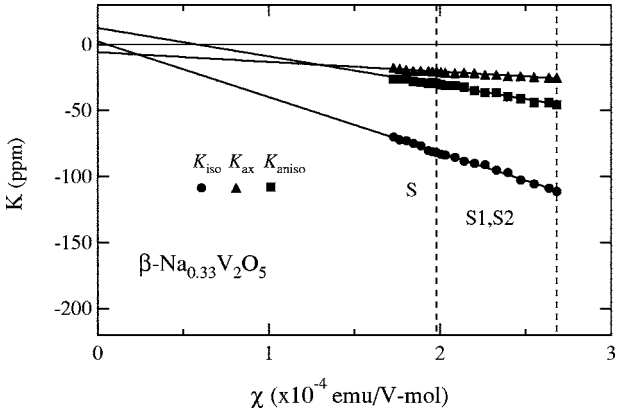

FIG. 10. ^{23}Na Knight shifts versus magnetic susceptibility plots as temperature as an implicit parameter in the metallic phases of β-$Na_{0.33}V_2O_5$.

above (below) T_{Na} correspond to the positions along the a axis, $x/a \sim 0$ and 1/2 (1/4 and 3/4), respectively. Also mirror planes, glide planes, twofold screw axes, twofold rotation axes, and inversion centers are presented.[12,24] The origins in Figs. 11(b) and 11(c) are shifted to $(a/4, b/4, 0)$ due to the change of the crystal symmetry.

Above T_{Na}, there are four Na positions, Na(1)–Na(4), in the unit cell as seen in Fig. 11(a) where the mirror planes, glide planes, twofold rotation axes, twofold screw axes, and inversion centers are also shown. In particular, the ca^* plane with the mirror symmetry at the Na site results in that the b axis is one of the principal axes of the EFG tensor. The four Na positions are randomly occupied by Na atoms, leading to

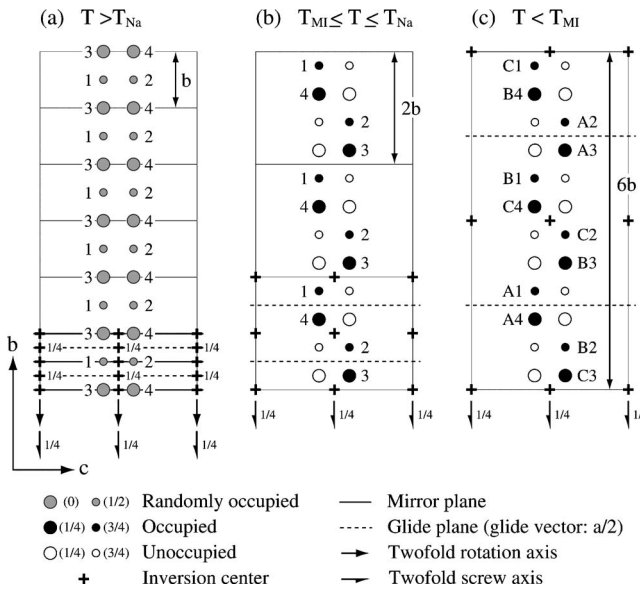

FIG. 11. Projection of the Na sites on the bc plane for (a) $T > T_{Na}$, (b) $T_{MI} \leqslant T \leqslant T_{Na}$, and (c) $T < T_{MI}$ in β-$Na_{0.33}V_2O_5$. The gray circles are randomly occupied by Na atoms, whereas the black and white ones are occupied and unoccupied, respectively. The large and small circles above (below) T_{Na} correspond to the positions along the a axis, $x/a \sim 0$ and 1/2 (1/4 and 3/4), respectively. Mirror planes, glide planes, twofold rotation axes, twofold screw axes, and inversion centers are also presented in the unit cells.

the Na positions which are equivalent from the crystallographic point of view. This is a reason why we observed one NMR spectrum as seen in Fig. 2.

The Na ordering takes place and the lattice constant along the b axis becomes $2b$ in the T range $T_{MI} \leqslant T \leqslant T_{Na}$. Consequently, the ca^* plane loses the mirror symmetry for the Na sites and the twofold rotation axes are also lost, while the glide planes, twofold screw axes, and inversion centers remain as shown in Fig. 11(b). This fact is expected to result in the Na(1) and Na(3) positions have the EFG axes with different directions from those of Na(2) and Na(4). This was observed as seen in Fig. 3 where there are two sets of ^{23}Na NMR spectra for the H_0 rotation in the bc and a^*b planes, and also all the Na(1)–Na(4) positions lead to one set of ^{23}Na spectrum for $H_0 \perp b$ and $H_0 \| b$.

The lattice modulation of $6b$ along the b axis, which is attributed to the CO or the CD accompanied by the MI transition, appears below T_{MI}. Consequently, there are three crystallographically inequivalent sites Na(A), Na(B), and Na(C) sites. Each site Na(P) (P=A, B, and C) has four positions Na($P1$)–Na($P4$) as shown in Fig. 11(c). There are also the glide planes, twofold screw axes, and inversion centers. Due to these site symmetries, the directions of the principal axes of the EFG tensor at Na($P1$) [Na($P2$)] are expected to coincide with those at Na($P3$) [Na($P4$)], whereas the directions at Na($P1$) are different from those at Na($P2$). Also ^{23}Na NMR spectra coming from Na($P1$) and Na($P3$) are equivalent to spectra from Na($P2$) and Na($P4$) for $H_0 \perp b$ and $H_0 \| b$. Therefore we observed six sets of NMR spectra for H_0 rotation in the bc and a^*b planes, and three sets for $H_0 \perp b$ and $H_0 \| b$ in the T range $T_N < T < T_{MI}$ as seen in Fig. 4.

Thus we can conclude that the ^{23}Na NMR spectra observed in the present experiment are consistent with the lattice symmetry proposed by the x-ray diffraction[11] and neutron scattering[12] studies.

B. Charge disproportionation

We can obtain information on the pattern of the CO or the CD from the Knight shift. A Na^+ ion in a tunnel of the V_2O_5 framework is considered to interact with the magnetic moments at the vanadium sites dominantly via a classical dipole interaction, leading to the anisotropy of the observed Knight shift. The T-dependent K_{iso} observed, however, indicates the presence of a transferred hyperfine interaction may be due to mixing between Na s and V d orbitals. The fraction of the mixing is roughly estimated to be small, ~0.04%, from comparing the observed value of $|A_{hf}^{iso}| = 2.35$ kOe/μ_B with the hyperfine coupling constant of ~6100 kOe/μ_B calculated for the s orbital.[25] Therefore, the mixing of the Na p and V d orbitals should be negligibly small as well as the mixing of the Na s and V d orbitals, even if the mixing may be present. Thus the anisotropy of K is governed by the dipole interaction. The Knight shift due to the dipole interaction, K_{dip}, is expressed as follows:

$$K_{dip} = \sum_j \chi_j \frac{3(\mathbf{n_0} \cdot \mathbf{r}_j)^2 - r_j^2}{r_j^5}, \tag{7}$$

where χ_j is the local magnetic susceptibility of the jth V lattice site, $\mathbf{r}_j$ is a vector connecting the Na site in concern to the jth V lattice site, $\mathbf{n_0}$ is the unit vector of the external field, and the summation is taken over the V lattice sites in a sphere with a radius of 200 Å. In the calculation of K_{dip} at 300, 150, and 40 K, we used the crystal structure data at 293, 150, and 90 K, respectively, determined by Yamaura *et al.*[26] which were confirmed by neutron scattering measurements.[12]

First, we analyze the experimental data of ^{23}Na Knight shift K at 150 K in the metallic phase with the Na ordering. Recently, ^{51}V NMR measurements have enabled us to know the local magnetic properties in the metallic phases of β-$Na_{0.33}V_2O_5$, particularly, that the V1 site is the most magnetic.[15] As mentioned above, each V site has two crystallographically inequivalent sites V(A) and V(B) in the T range $T_{MI} \leqslant T \leqslant T_{Na}$. There is a slight difference between χ[V3(A)] and χ[V3(B)], and no difference between χ[V2(A)] and χ[V2(B)] as revealed by the ^{51}V NMR measurements.[15] The local magnetic susceptibilities were also estimated as $\chi(V1) = 4.8 \times 10^{-4}$ emu/V1-mol, $\chi(V2) = 1.3 \times 10^{-4}$ emu/V2-mol, and $\chi(V3) = 1.5 \times 10^{-4}$ emu/V3-mol at 150 K where the χ(V3) value is the average of χ[V3(A)] and χ[V3(B)]. Using Eq. (7) and the above estimated susceptibilities for the model M1 with the most magnetic V1 site as presented in Fig. 12(a), we calculated the angular dependence of K_{dip}, which does not contribute to K_{iso}, as presented in Fig. 13. Also the calculated curves for the model M2 (M3), where the V2 (V3) site is the most magnetic, with $\chi(V1) = 1.5(1.5) \times 10^{-4}$ emu/V1-mol, $\chi(V2) = 4.8(1.3) \times 10^{-4}$ emu/V2-mol, and $\chi(V3) = 1.3(4.8) \times 10^{-4}$ emu/V3-mol as shown in Fig. 12(b) [Fig. 12(c)] are also presented for comparison. The shift K_{dip} at the Na(1) and Na(3) positions coincides with that at the Na(2) and Na(4) positions, although the EFG tensors are different from each other. As seen in Fig. 13, the model M1 can well reproduce the experimental data of $K - K_{iso}$ in the ca^* plane where K_{iso} listed in Table II is subtracted from K, whereas the other models cannot explain them. Similarly we make an analysis of the experimental results at 300 K using the model M4 with $\chi(V1) = 2.6 \times 10^{-4}$ emu/V1-mol, $\chi(V2) = 1.5 \times 10^{-4}$ emu/V2-mol, and $\chi(V3) = 1.0 \times 10^{-4}$ emu/V3-mol determined by the ^{51}V NMR study[15] as shown in Fig. 14(a). The calculated results are presented in Fig. 14 with the experimental results of $K - K_{iso}$. The experimental results are well reproduced by this model. Thus we can clearly conclude that the V1 site is the most magnetic in the metallic phases, and this conclusion yields the validity to the ^{51}V NMR analysis of the local magnetic susceptibilities.[15]

In the insulating phase, several CO models of V^{4+} and V^{5+} have been proposed. In early studies the chain models with V^{4+} located at half of the V1 or V2 sites and the zigzag model with V^{4+} at the V2 sites were taken into account.[16,17] After these studies, however, the x-ray diffraction measurements revealed that the CO pattern has the $6b$ lattice modulation along the b axis.[11] Therefore the models without the $6b$ modulation can be rejected. Up to now, three models have been mainly proposed as a model of the CO or the CD pattern in β-$Na_{0.33}V_2O_5$. In the insulating phase there exist six crystallographically inequivalent V sites denoted by A-F at each V site. Yamaura *et al.* proposed the model I1 of the rectangular type CO pattern with V^{4+} located at the V2(D),

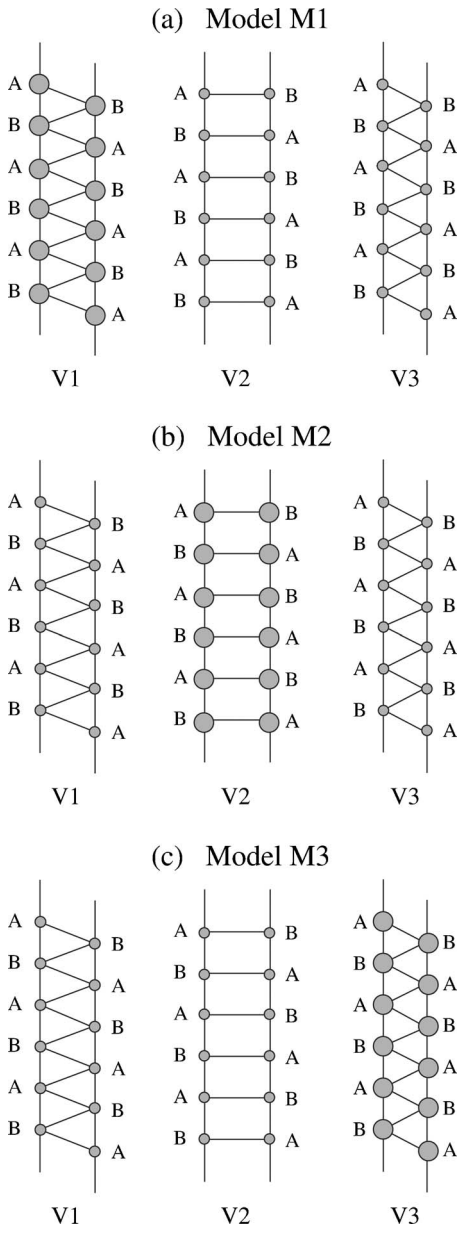

FIG. 12. Models (a) M1, (b) M2, and (c) M3 of the distribution of the local magnetic susceptibilities at the V1, V2, and V3 sites in the metallic phase of β-$Na_{0.33}V_2O_5$ with the Na ordering. The ratio of the size of the gray circles corresponds to that of the local magnetic susceptibilities $\chi(V1):\chi(V2):\chi(V3)=4.8:1.3:1.5$, 1.5:4.8:1.3, and 1.5:1.3:4.8 for the models M1, M2, and M3, respectively, at 150 K.

V2(E), and V2(F) sites, and V^{5+} at the other V sites as shown in Fig. 15(a).[11] From ESR experiments Heinrich *et al.* also discussed the model I2 that the V1(C), V1(D), and V1(E) sites are occupied by V^{4+} as shown in Fig. 16(a).[19] Recently, Nagai *et al.* proposed the spin structure in the AF state with magnetic moments of 3.2, 1.8, and 3.3 μ_B which are summed up for all the V1, V2, and V3 sites, respectively, in the unit cell of $a\times 6b\times c$.[12] The magnetic moments are located at the VS(B), VS(C), VS(E), and VS(F) (S=1, 2, and 3) sites, whereas the VS(A) and VS(D) sites are occupied by nonmagnetic V^{5+}. This naturally leads to the model

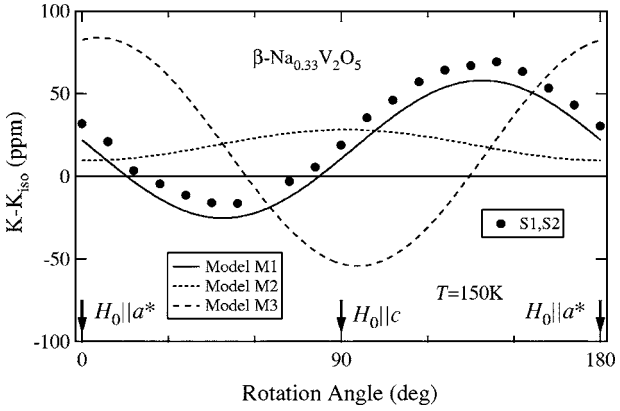

FIG. 13. Angular dependence of $K-K_{iso}$ of the ^{23}Na NMR spectra, S1 and S2, at 150 K with H_0 rotated in the ca^* plane of β-$Na_{0.33}V_2O_5$. The solid, dotted, and dashed curves represent the theoretical results due to the dipole interaction calculated for the models, M1–M3, respectively (see Fig. 12).

I3 shown in Fig. 17(a) where the magnetic V1, V2, and V3 sites in the paramagnetic insulating phase have magnetic susceptibilities such as $\chi(V1):\chi(V2):\chi(V3)=3.2:1.8:3.3$. We calculate K_{dip} based on the models I1–I3 and the value of $\chi=3.8\times10^{-4}$ emu/V-mol at 40 K (Ref. 15) and compare the calculated results of the angular dependence of K with the experimental data at 40 K. Figure 15 (16) shows the calculated result, for example, in the ca^* (a^*b) plane based on the model I1 (I2). The three curves in the ca^* plane and the six curves in the a^*b plane come from the Na(A), Na(B), and Na(C) sites with the 1–4 positions as discussed in the Sec. IV A. These calculated curves based on both models cannot reproduce the experimental results. The model I3 explains relatively well the angular dependences of K in the bc and a^*b planes as seen in Fig. 17, whereas the ca^* data cannot be done. After looking for various models to reproduce the angular dependence of $K-K_{iso}$ at 40 K, we finally found the most suitable one I4 having the distribution of magnetic moments with $\chi(V1):\chi(V2):\chi(V3)=3:1:1$ similar to the model I3 as shown in Fig. 18. The calculated curves of the angular dependence of $K-K_{iso}$ based on the model I4 reproduce the overall angular dependences of $K-K_{iso}$. The slight deviation between the calculated and experimental results may come from the T dependence of the lattice positions, the estimation of the magnetic moment at each V site, and so on. This K measurement is a direct observation of the charge distribution in the insulating phase of β-$Na_{0.33}V_2O_5$. Thus the present NMR results clearly reveal that the MI transition is accompanied not by the CO of V^{4+} and V^{5+} but by the CD.

C. Spin structure in the antiferromagnetic state

Based on the model I4 and the ^{51}V NMR spectra under zero external field in the AF state, we discuss the spin structure in the AF state of β-$Na_{0.33}V_2O_5$. In the NMR spectra at 1.5 K, ^{51}V resonance lines were observed at 0.1, 17.9, 30.3, and 81.0 MHz which correspond to the internal fields H_n of 0.1, 16.0, 27.1, and 72.4 kOe, respectively.[16] The d_{xy} type

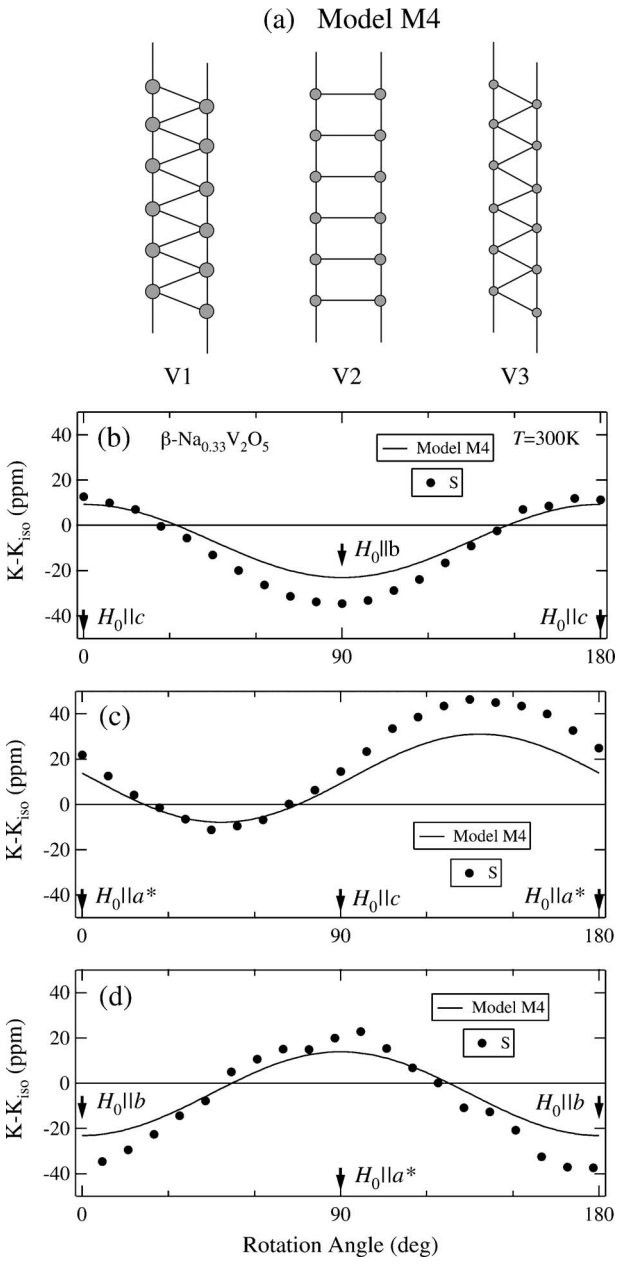

FIG. 14. (a) Model M4 of the distribution of the local magnetic susceptibilities at the V1, V2, and V3 sites in the metallic phase of β-$Na_{0.33}V_2O_5$ without the Na ordering. The ratio of the size of the gray circles corresponds to that of the magnetic susceptibilities $\chi(V1):\chi(V2):\chi(V3)=2.6:1.5:1.0$ at 300 K. Angular dependence of $K-K_{iso}$ of the ^{23}Na NMR spectrum, S, at 300 K with H_0 rotated in the (b) bc, (c) ca^*, and (d) a^*b planes of β-$Na_{0.33}V_2O_5$. The solid curves represent the theoretical results due to the dipole interaction calculated for the model M4.

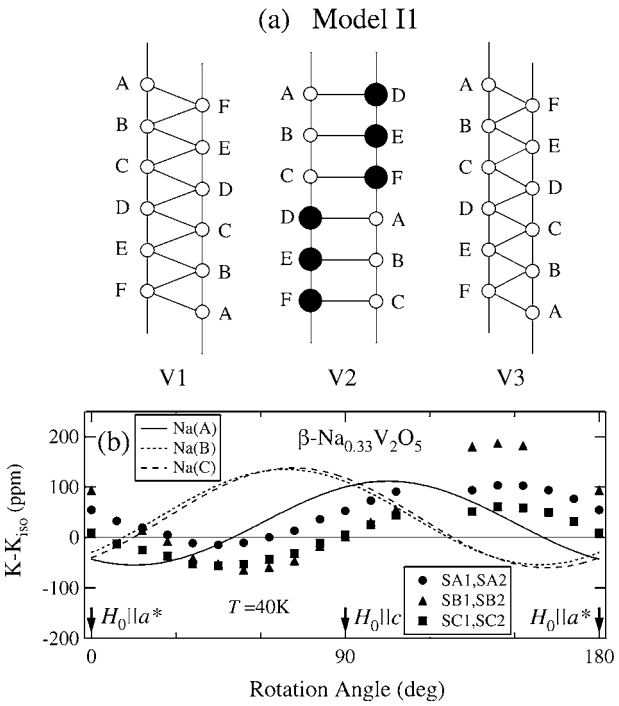

FIG. 15. (a) Model I1 of the charge ordering pattern proposed from the x-ray diffraction study (Ref. 11) in the insulating phase of β-$Na_{0.33}V_2O_5$. The black and white circles represent the V^{4+} and V^{5+} sites, respectively. (b) Angular dependence of the ^{23}Na Knight shift $K-K_{iso}$ in the ca^* plane calculated for the model I1 at 40 K in β-$Na_{0.33}V_2O_5$. The solid, dotted, and dashed curves denote the calculated results for the Na(A), Na(B), and Na(C) sites, respectively, whereas the solid symbols represent experimental data.

orbital, which was estimated to be a singlet orbital ground state from the crystal field calculation[15] as shown in Fig. 19, results in no orbital hyperfine field. Also the small deviation of the electron g value from two observed in the ESR experiment[19] enables us to neglect the hyperfine field due to the spin-orbit interaction. Thus H_n is mainly ascribed to the Fermi-contact field, H_F, due to the core-polarization effect and the dipole field, H_{dip}, coming from a $3d$ electron on the magnetic V ions. The coupling constant of H_F is generally expressed as $A_F=\kappa\mu_B\langle r^{-3}\rangle$ where $\langle r^{-3}\rangle$ is the average value of r^{-3} for the d orbital and κ is a parameter of the Fermi contact interaction due to the core polarization effect, whereas the coupling constants due to the dipole interaction parallel and perpendicular to the z axis are expressed as $A_{dip}^{\parallel}=-\frac{4}{7}\mu_B\langle r^{-3}\rangle$ and $A_{dip}^{\perp}=\frac{2}{7}\mu_B\langle r^{-3}\rangle$, respectively, for the d_{xy} orbital.[27] Therefore, H_n is written by

$$H_n = Mk\sqrt{(A_F + A_{dip}^{\parallel})^2\cos^2\theta_n + (A_F + A_{dip}^{\perp})^2\sin^2\theta_n}, \quad (8)$$

where θ_n is the angle between the z axis of the d_{xy} orbital and the spin moment M, and k is a reduction parameter of $\langle r^{-3}\rangle$ due to the covalent effect. In transition metal oxides with a $3d^1$ configuration, $A_F\sim-100$ kOe/μ_B (Ref. 28), whereas $A_{dip}^{\parallel}$ ($A_{dip}^{\perp}$) is calculated to be -130 (65) kOe/μ_B from the Hartree-Fock value of $\langle r^{-3}\rangle=3.684$ atomic units.[27] If M at all the VS(B), VS(C), VS(E), and VS(F) sites are 0.45, 0.15, and 0.15 μ_B for S=1, 2, and 3, respectively, which are based on the proposed model I4, and $k=0.8$, H_n at the magnetic V1 (V2 and V3) sites are in the range of 13 kOe$\leqslant H_n \leqslant$83 kOe (4.2 kOe$\leqslant H_n \leqslant$28 kOe) and dependent on θ_n. If H_n at the magnetic V1, V2, and V3 sites are 72.4, 16.0, and 27.1 kOe, respectively, we obtain $\theta_n=29°$, 56°, and 11° for the V1, V2, and V3 sites, respectively. This result is shown in Fig. 19 where the directions of the spin moments between the neighboring sites follow the neutron scattering result.[12]

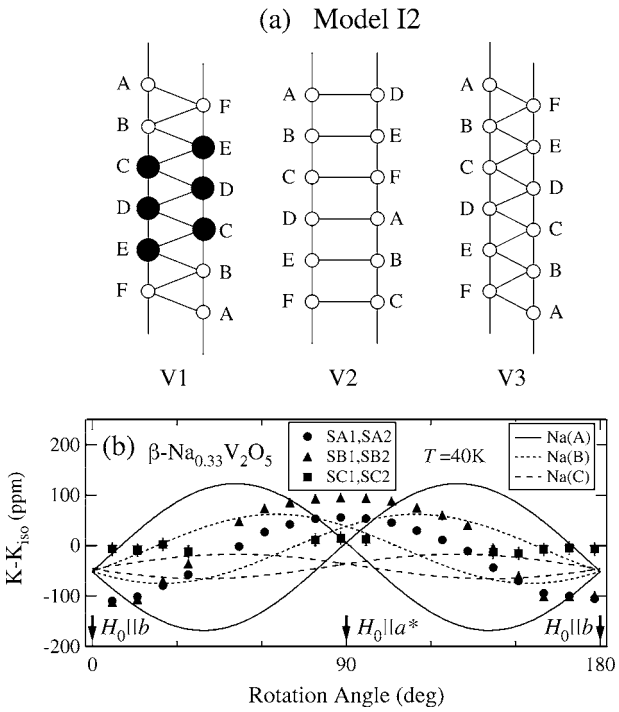

FIG. 16. (a) Model I2 of the charge ordering pattern proposed from the ESR study (Ref. 19) in the insulating phase of β-$Na_{0.33}V_2O_5$. The black and white circles represent the V^{4+} and V^{5+} sites, respectively. (b) Angular dependence of the ^{23}Na Knight shift $K-K_{iso}$ in the a^*b plane calculated for the model I2 at 40 K in β-$Na_{0.33}V_2O_5$. The solid, dotted, and dashed curves denote the calculated results for the Na(A), Na(B), and Na(C) sites, respectively, whereas the solid symbols represent experimental data.

The other nonmagnetic V sites, VS(A) and VS(D) (S=1, 2, and 3), provide the NMR line with H_n=0.1 kOe. This spin structure is consistent with the model proposed by the neutron scattering study except the spin amplitude at the three vanadium sites. Thus the model I4 can well reproduce the ^{51}V NMR lines observed under zero external field in the AF state of β-$Na_{0.33}V_2O_5$.

D. Electronic structure and metal-insulator transition

We discuss the electronic structure of β-$Na_{0.33}V_2O_5$. Recently, based on vanadyl bond orientation and extended Hückel tight-binding calculations, Doublet and Lepetit proposed a model of weakly interacting two-leg ladders composed of one V2-V2 and two V1-V3 ladders for β-$Sr_{0.33}V_2O_5$, in contrast with a model with two zigzag chains and one two-leg ladder.[14] In this model, the nearest and the second nearest V2-V2 interactions form the V2-V2 ladders represented by the solid lines as shown in Fig. 20, whereas the nearest V1-V3, the second nearest V1-V1, and the second nearest V3-V3 interactions form the V1-V3 ladders. These V2-V2 and V1-V3 ladders are coupled by weak interactions denoted by the dotted lines. This model is based on the orbital ordering of each V site shown in Fig. 19. In the ^{51}V NMR study, based on this model and the analysis of the local magnetic susceptibilities, we proposed the model of the weakly interacting two-leg ladders with the electron numbers

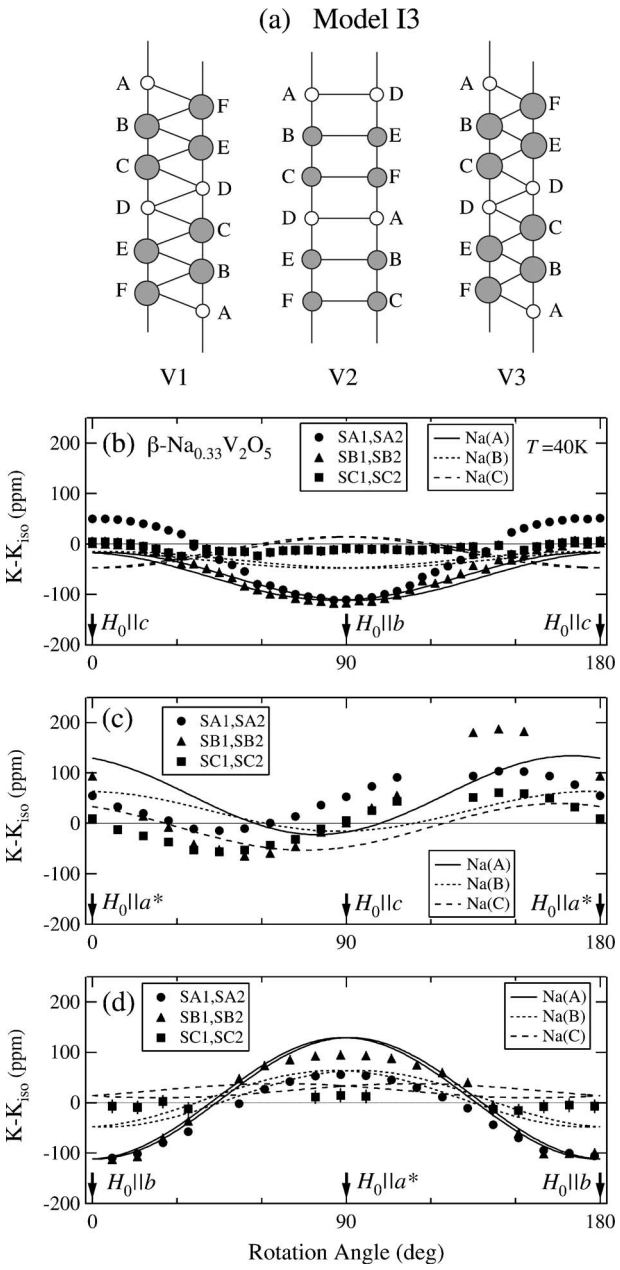

FIG. 17. (a) Model I3 of the charge disproportionation pattern inferred from the neutron scattering study (Ref. 12) in the insulating phase of β-$Na_{0.33}V_2O_5$. The ratio of the size of the gray circles corresponds to that of magnetic susceptibilities $\chi(V1):\chi(V2):\chi(V3)=3.2:1.8:3.3$, whereas the open circles denote V^{5+}. Angular dependence of the ^{23}Na Knight shift $K-K_{iso}$ in the (b) bc, (c) ca^*, and (d) a^*b planes calculated for the model I3 at 40 K in β-$Na_{0.33}V_2O_5$. The solid, dotted, and dashed curves denote the calculated results for the Na(A), Na(B), and Na(C) sites, respectively, whereas the solid symbols represent experimental data.

given below as a model of the electronic structure in the metallic phases without and with the Na ordering.[15] That is, the V1, V2, and V3 sites on the ladders have 3d electron numbers of about 0.25, 0.14, and 0.11 electron/V-ion, respectively, for $T>T_{Na}$. In the T range $T_{MI}\leqslant T\leqslant T_{Na}$, the modulation along the b axis slightly takes place. These electron numbers at the V sites are supported by the present ^{23}Na

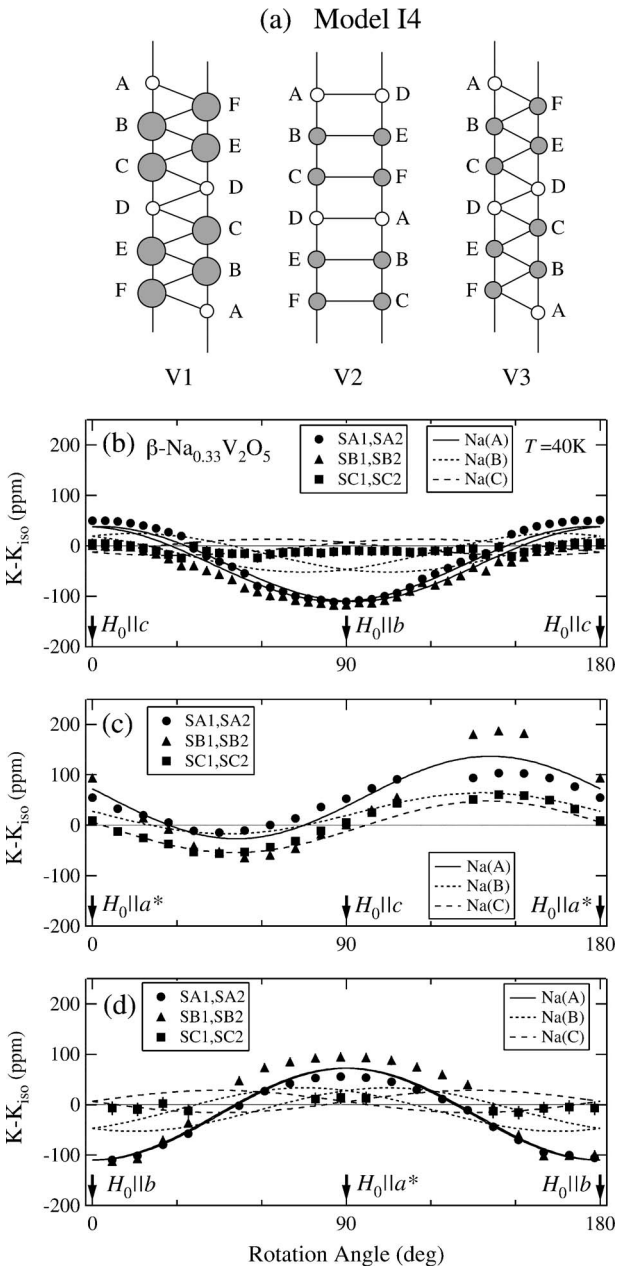

FIG. 18. (a) Model I4 of the charge disproportionation pattern in the insulating phase of β-$Na_{0.33}V_2O_5$. The ratio of the size of the gray circles corresponds to that of magnetic susceptibilities $\chi(V1):\chi(V2):\chi(V3)=3:1:1$, whereas the open circles denote V^{5+}. Angular dependence of the ^{23}Na Knight shift $K-K_{iso}$ in the (b) bc, (c) ca^*, and (d) a^*b planes calculated for the model I4 at 40 K in β-$Na_{0.33}V_2O_5$. The solid, dotted, and dashed curves denote the calculated results for the Na(A), Na(B), and Na(C) sites, respectively, whereas the solid symbols represent experimental data.

NMR study discussed in the Sec. IV B. Furthermore, the present study naturally leads to the model below T_{MI} as shown in Fig. 20, that is, 3d electrons are located on the magnetic VS(B), VS(C), VS(E), and VS(F) (S=1, 2, and 3) sites with the electron numbers of about 0.45, 0.15 and 0.15 electron/V-ion, respectively, whereas the VS(A) and VS(D) sites are occupied by nonmagnetic V^{5+} with no 3d electron.

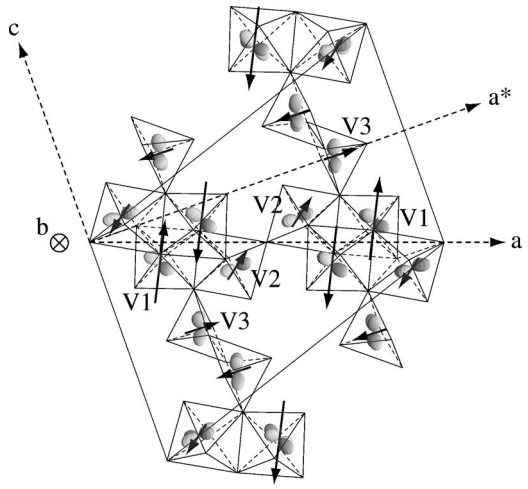

FIG. 19. Spin structure of the magnetic sites in the antiferromagnetic state of β-$Na_{0.33}V_2O_5$. The solid arrows represent the spin moments. The 3d electron orbitals at the V1, V2, and V3 sites based on the crystal field calculation (Ref. 15) are also shown.

Based on the model of the electronic structure mentioned above, we discuss the electron filling and the mechanism of the MI transition accompanied by the CD. Doublet and Lepetit calculated the hopping energies of the rungs and the legs, $t_\perp$ and $t_\parallel$, respectively, in the V2-V2 and V1-V3 ladders of β-$Sr_{0.33}V_2O_5$.[14] They obtained $t_\perp=-0.203\sim-0.237$ and $t_\parallel=-0.140\sim-0.173$ eV in the V1-V3 ladder, and $t_\perp=-0.313$ and $t_\parallel=-0.135\sim-0.147$ eV in the V2-V2 ladder, whereas the interladder hoping energies are much smaller than the intraladder energies. This anisotropy of the hopping energies is seen in the high temperature phase of α'-NaV_2O_5 (Ref. 29). The bonding orbital of the intraladder is considered to be occupied, whereas the antibonding is empty. Conse-

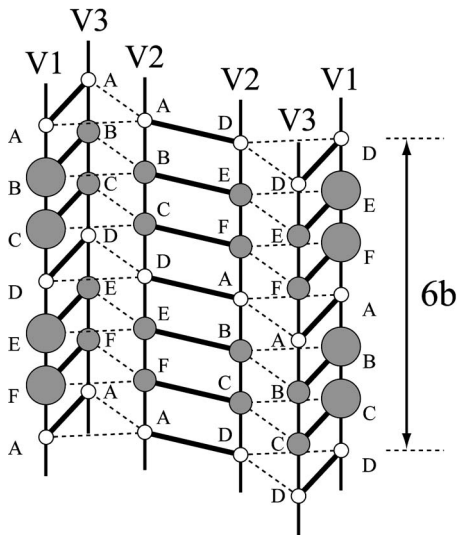

FIG. 20. Schematic structure of interactions and electron number at the V1(A)-V1(F), V2(A)-V2(F), and V3(A)-V3(F) sites below T_{MI} in β-$Na_{0.33}V_2O_5$. The magnetic sites are represented by the gray circles with the size proportional to the 3d electron number, whereas the open circles denote V^{5+} sites with no 3d electron.

quently the quarter-filled ladder effectively behaves as a half-filled chain in α'-NaV_2O_5. If the V2-V2 (V1-V3) ladder with the $3d$ electron numbers of 0.25, 0.14, and 0.11 electron/V-ion at the V1, V2, and V3 sites, respectively, in β-$Na_{0.33}V_2O_5$ may similarly behave as a one-dimensional chain, $k_F=0.14\pi/b$ $(0.18\pi/b)$ where k_F is the Fermi wave vector. However, this is not consistent with a fact that the maximum intensity is observed at $k\sim\pm\pi/4b$ in the metallic phase in the angle-resolved photoemission spectroscopy measurement.[13] This may indicate that the intersite hopping energies between the two-leg ladders cannot be neglected. In addition to these interactions, onsite and intersite Coulomb energies should be taken into account. Furthermore, the quasi-one-dimensional structure leads to a quasi-one-dimensional band structure where a large nesting on the Fermi surface is expected.[30] At the same time, the nesting on the Fermi surface and an electron-phonon interaction seems to result in a Peierls-type instability which leads to the MI transition and the CD observed in the present NMR experiments. Thus the appearance of the $3b$ modulation not with the CO of V^{4+} and V^{5+} but with the CD naturally may lead to the charge density wave state proposed by the nonlinear transport measurement.[31,32] Recently, a pressure-induced dimensional crossover and the relevance of the electron-phonon coupling in β-$Na_{0.33}V_2O_5$ were inferred, and the possibility of the polaronic quasiparticles for the superconductivity was discussed from the infrared reflectivity measurement under high pressure.[33] The superconductivity observed under high pressure in β-$Na_{0.33}V_2O_5$ may be related to the superconductivity, which appears under the pressure range of 3–8 GPa with a transition temperature passing through a maximum at 10 K around 4 GPa, in the quasi-one-dimensional ladder compound $Sr_{14-x}Ca_xCu_{24}O_{41}$ with $x\sim12$.[34] Also the superconducting mechanism has been intensively discussed for the hole-doped two-leg ladder system.[35,36] Thus the ladder structure seems to play an important role for the superconductivity in β-$Na_{0.33}V_2O_5$ as well as in $Sr_{14-x}Ca_xCu_{24}O_{41}$. The model of the weakly coupled ladders with the small electron filling proposed in the present study is a starting model to understand the electronic, magnetic, and superconducting properties of β-$Na_{0.33}V_2O_5$. Theoretical studies based on this model are highly desired to explain the mechanisms of the MI transition and the superconductivity in β-$Na_{0.33}V_2O_5$.

V. SUMMARY

We have made ^{23}Na NMR measurements on a single crystal to study the charge disproportionation and the metal-insulator transition in β-$Na_{0.33}V_2O_5$. We determined in detail the electric field gradient tensors at the Na sites in the metallic and insulating phases of β-$Na_{0.33}V_2O_5$. Comparing the EFG tensors with the site symmetry, we concluded that the EFG tensors are consistent with the space groups proposed by x-ray diffraction and neutron scattering studies. We determined ^{23}Na Knight shifts and compared the anisotropy of the Knight shifts with the calculated one due to the dipole field from the vanadium magnetic moments based on several models of the charge ordering and the charge disproportionation. We concluded that the V1 site is the most magnetic and that the metal-insulator transition is accompanied not by the charge ordering of V^{4+} and V^{5+} but by the charge disproportionation with the $3b$ modulation. We proposed the weakly coupled V2-V2 and V1-V3 ladders as a model of the electronic structure in the metallic and insulating phases and discussed the metal-insulator transition on the basis of the model.

ACKNOWLEDGMENTS

The authors would like to thank S. Nagai, M. Isobe, K. Okazaki, and M. Tsuchiizu for fruitful discussions, and S. Inoue for technical assistance. This study was supported by a Grant-in-Aid for Scientific Research from the Japan Society for the Promotion of Science.

[1] M. Imada, A. Fujimori, and Y. Tokura, Rev. Mod. Phys. **70**, 1039 (1998).
[2] M. Isobe and Y. Ueda, J. Phys. Soc. Jpn. **65**, 1178 (1996).
[3] H. Seo and H. Fukuyama, J. Phys. Soc. Jpn. **67**, 2602 (1998).
[4] T. Yamauchi, Y. Ueda, and N. Môri, Phys. Rev. Lett. **89**, 057002 (2002).
[5] Y. Ueda, M. Isobe, and T. Yamauchi, J. Phys. Chem. Solids **63**, 951 (2002).
[6] T. Yamauchi, M. Isobe, and Y. Ueda, Solid State Sci. **7**, 874 (2005).
[7] H. Yamada and Y. Ueda, J. Phys. Soc. Jpn. **68**, 2735 (1999).
[8] M. Itoh, N. Akimoto, H. Yamada, M. Isobe, and Y. Ueda, Physica C **341**, 2133 (2000).
[9] A. N. Vasil'ev, V. I. Marchenko, A. I. Smirnov, S. S. Sosin, H. Yamada, and Y. Ueda, Phys. Rev. B **64**, 174403 (2001).
[10] A. D. Wadsley, Acta Crystallogr. **8**, 695 (1955).
[11] J. Yamaura, M. Isobe, H. Yamada, T. Yamauchi, and Y. Ueda, J. Phys. Chem. Solids **63**, 957 (2002).
[12] S. Nagai, M. Nishi, K. Kakurai, Y. Oohara, H. Yoshizawa, H. Kimura, Y. Noda, B. Grenier, T. Yamauchi, J. Yamaura, M. Isobe, Y. Ueda, and K. Hirota, J. Phys. Soc. Jpn. **74**, 1297 (2005).
[13] K. Okazaki, A. Fujimori, T. Yamauchi, and Y. Ueda, Phys. Rev. B **69**, 140506(R) (2004).
[14] M. L. Doublet and M. B. Lepetit, Phys. Rev. B **71**, 075119 (2005).
[15] T. Suzuki, I. Yamauchi, M. Itoh, T. Yamauchi, and Y. Ueda, Phys. Rev. B **73**, 224421 (2006).
[16] M. Itoh, N. Akimoto, H. Yamada, M. Isobe, and Y. Ueda, J. Phys. Soc. Jpn. Suppl. B **69**, 155 (2000).
[17] M. Itoh, N. Akimoto, H. Yamada, M. Isobe, and Y. Ueda, J. Phys. Chem. Solids **62**, 351 (2001).
[18] S. Nishimoto and Y. Ohta, J. Phys. Soc. Jpn. **70**, 309 (2001).
[19] M. Heinrich, H.-A. Krug von Nidda, R. M. Eremina, A. Loidl,

Ch. Helbig, G. Obermeier, and S. Horn, Phys. Rev. Lett. **93**, 116402 (2004).
[20] V. Ta Phuoc, C. Sellier, and E. Janod, Phys. Rev. B **72**, 035120 (2005).
[21] A. Abragam, *The Principles of Nuclear Magnetism* (Clarendon, Oxford, 1961).
[22] G. M. Volkoff, H. E. Petch, and D. W. Smellie, Can. J. Phys. **30**, 270 (1952).
[23] G. M. Volkoff, Can. J. Phys. **31**, 820 (1953).
[24] *International Table for Crystallography*, edited by Th. Hahn (Kluwer Academic, Dordrecht, 2002), vol. A.
[25] R. G. Shulman and V. Jaccarino, Phys. Rev. **108**, 1219 (1957).
[26] J. Yamaura, M. Isobe, T. Yamauchi, and Y. Ueda (unpublished).
[27] A. Abragam and B. Bleaney, *Electron Paramagnetic Resonance of Transition Ions* (Clarendon, Oxford, 1970).
[28] T. Kiyama, H. Saitoh, M. Itoh, K. Kodama, H. Ichikawa, and J. Akimitsu, J. Phys. Soc. Jpn. **74**, 1123 (2005).
[29] H. Smolinski, C. Gros, W. Weber, U. Peuchert, G. Roth, M. Weiden, and C. Geibel, Phys. Rev. Lett. **80**, 5164 (1998).
[30] G. Obermeier, D. Ciesla, S. Klimm, and S. Horn, Phys. Rev. B **66**, 085117 (2002).
[31] S. Sirbu, T. Yamauchi, Y. Ueda, and P. H. M. van Loosdrecht, J. Phys. IV **131**, 115 (2005).
[32] S. Sirbu, P. H. M. van Loosdrecht, T. Yamauchi, and Y. Ueda, cond-mat/0512080 (unpublished).
[33] C. A. Kuntscher, S. Frank, I. Loa, K. Syassen, T. Yamauchi, and Y. Ueda, Phys. Rev. B **71**, 220502(R) (2005).
[34] T. Nagata, M. Uehara, J. Goto, J. Akimitsu, N. Motoyama, H. Eisaki, S. Uchida, H. Takahashi, T. Nakanishi, and N. Môri, Phys. Rev. Lett. **81**, 1090 (1998).
[35] E. Dagotto, J. Riera, and D. Scalapino, Phys. Rev. B **45**, R5744 (1992).
[36] M. Sigrist, T. M. Rice, and F. C. Zhang, Phys. Rev. B **49**, 12058 (1994).